nature physics

ARTICLES

https://doi.org/10.1038/s41567-020-01055-5

Directional self-locomotion of active droplets enabled by nematic environment

Mojtaba Rajabi[1,3], Hend Baza[1,3], Taras Turiv[2] and Oleg D. Lavrentovich[1,2]✉

Active matter composed of self-propelled interacting units holds a major promise for the extraction of useful work from its seemingly chaotic dynamics. Streamlining active matter is especially important at the microscale, where the viscous forces prevail over inertia and transport requires a non-reciprocal motion. Here we report that microscopic active droplets representing aqueous dispersions of swimming bacteria *Bacillus subtilis* become unidirectionally motile when placed in an inactive nematic liquid-crystal medium. Random motion of bacteria inside the droplet is rectified into a directional self-locomotion of the droplet by the polar director structure that the droplet creates in the surrounding nematic through anisotropic molecular interactions at its surface. Droplets without active swimmers show no net displacement. The trajectory of the active droplet can be predesigned by patterning the molecular orientation of the nematic. The effect demonstrates that broken spatial symmetry of the medium can be the reason for and the means to control directional microscale transport.

Active droplets are spatially restricted fluid volumes containing self-propelled and interacting units. They are gaining an increasing interest as a model system[1–14] to understand the dynamics of microscopic organisms that developed sophisticated modes of propulsion and self-replication. Self-propulsion at microscales is peculiar since viscosity prevails over inertia, and microorganisms should use non-reciprocal modes of movement, such as rotation of a flagellum[15]. Another challenge is maintaining a certain direction of propulsion[16]. Most living and synthetic microswimmers demonstrate an 'enhanced' version of the Brownian motion. At timescales shorter than the time of realignment by orientational fluctuations, the motion is directional, but at longer timescales it becomes diffusive with zero net displacements[16]. Such an enhanced Brownian motion was reported for active disk-like droplets of microtubules[2] and *Escherichia coli*-containing water droplets in an isotropic oil[14]. As stressed by Marchetti[17], an important challenge is to find a way to control the propulsion direction of active droplets. Extraction of work from active matter has been achieved for ratchet gears that rotate when placed in an active bacterial bath[18,19]; in contrast, a controllable rectilinear or curvilinear propulsion remains elusive.

Here we demonstrate controllable rectilinear and curvilinear propulsion of active droplets enabled by spatially broken symmetry of the local environment that the active droplet creates when placed in an orientationally ordered nematic fluid. The active droplets represent aqueous dispersions of motile bacteria *Bacillus subtilis*. These droplets are dispersed in an inactive hydrophobic thermotropic nematic and stabilized by a small amount of a surfactant (lecithin). The nematic is formed by anisotropic molecules aligned along a single non-polar direction $\hat{\mathbf{n}}$ $\left(\hat{\mathbf{n}} \equiv -\hat{\mathbf{n}},\ \hat{\mathbf{n}}^2 = 1\right)$, called the director[20]. Lecithin sets $\hat{\mathbf{n}}$ perpendicularly to the surface of the active droplets. To match the overall uniform alignment $\hat{\mathbf{n}}_0 =$ constant set by the bounding glass plates, each droplet acquires a satellite topological defect: either a point defect, the so-called hyperbolic hedgehog[21] (Fig. 1a–c) or an equatorial disclination ring resembling a Saturn ring[22,23] (Fig. 2a,b). We abbreviate these HH and SR configurations, respectively. The two differ dramatically in their symmetry and in impact on the dynamics of active droplets. The HH structure with a polar fore-aft asymmetric director deformation enables self-propulsion of the active droplets, by rectifying flows transferred from the active interior of the droplet to the inactive nematic environment. The SR of quadrupolar symmetry produces no net displacement, but once the SR shifts from the equatorial position towards one of the poles, the droplet becomes motile since the surrounding director field is no longer fore-aft symmetric. Without active bacteria, the droplets show no net displacement.

We use *B. subtilis*, a rod-shaped bacterium 5–7 μm long and ~0.7 μm in diameter. Two bacteria-containing active dispersions are explored: (1) an isotropic aqueous terrific broth (TB) and (2) a nematic lyotropic chromonic liquid crystal (LCLC), 13 wt% dispersion of disodium cromoglycate (DSCG) in TB. Bacterial concentrations $(5–20)c_0$, where $c_0 = 0.8 \times 10^{15}$ cell m^{-3}, are higher than the concentrations causing turbulent-like flows in aqueous[24,25] (~10^{15} m^{-3}) and LCLC dispersions[26] (~10^{14} m^{-3}) of *B. subtilis*. Emulsions of active droplets in the thermotropic nematic MAT-03-382 are filled into cells of thickness $d = 200$ μm, formed by two parallel glass plates with a unidirectional planar alignment, $\hat{\mathbf{n}}_0 = (1, 0, 0)$ in Cartesian coordinates.

The HH structure forms around droplets of diameter $10\,\mu\text{m} \leq 2R \leq 140\,\mu\text{m}$. In an infinite nematic, the HH structure is stable when the ratio $WR/K > 1$ (ref. [21]); W is the surface anchoring strength of perpendicular alignment and $K \approx 10$ pN is the average elastic constant[20]. Droplets smaller than some critical diameter $2R_c \approx 10$ μm do not form hedgehogs, which leads to an estimate $W \approx K/R_c \approx 10^{-6}$ J m^{-2}. Confinement by two flat plates favours the SR when the diameter approaches d (ref. [23]). We observe SRs around droplets with $80\,\mu\text{m} \leq 2R \leq 180\,\mu\text{m}$. The HH and SR configurations differ dramatically in their symmetry and in impact on the dynamics of active droplets.

The hedgehog structure is of a polar symmetry (Fig. 1a–c) and rectifies the chaotic motion of bacteria inside the droplet into polar locomotion of the droplet along the x axis (Fig. 1d–f). Both the LCLC-based (Fig. 1d) and isotropic droplets (Fig. 1e) propel with the hedgehog leading the way, with the velocity $\mathbf{v} = (v,0,0)$ (Supplementary Video 1). The distance r_d of the point defect from the centre of the drop fluctuates (Supplementary Fig. 1) within the

[1]Department of Physics, Kent State University, Kent, OH, USA. [2]Advanced Materials and Liquid Crystal Institute, Materials Science Graduate Program, Kent State University, Kent, OH, USA. [3]These authors contributed equally: Mojtaba Rajabi, Hend Baza. ✉e-mail: olavrent@kent.edu

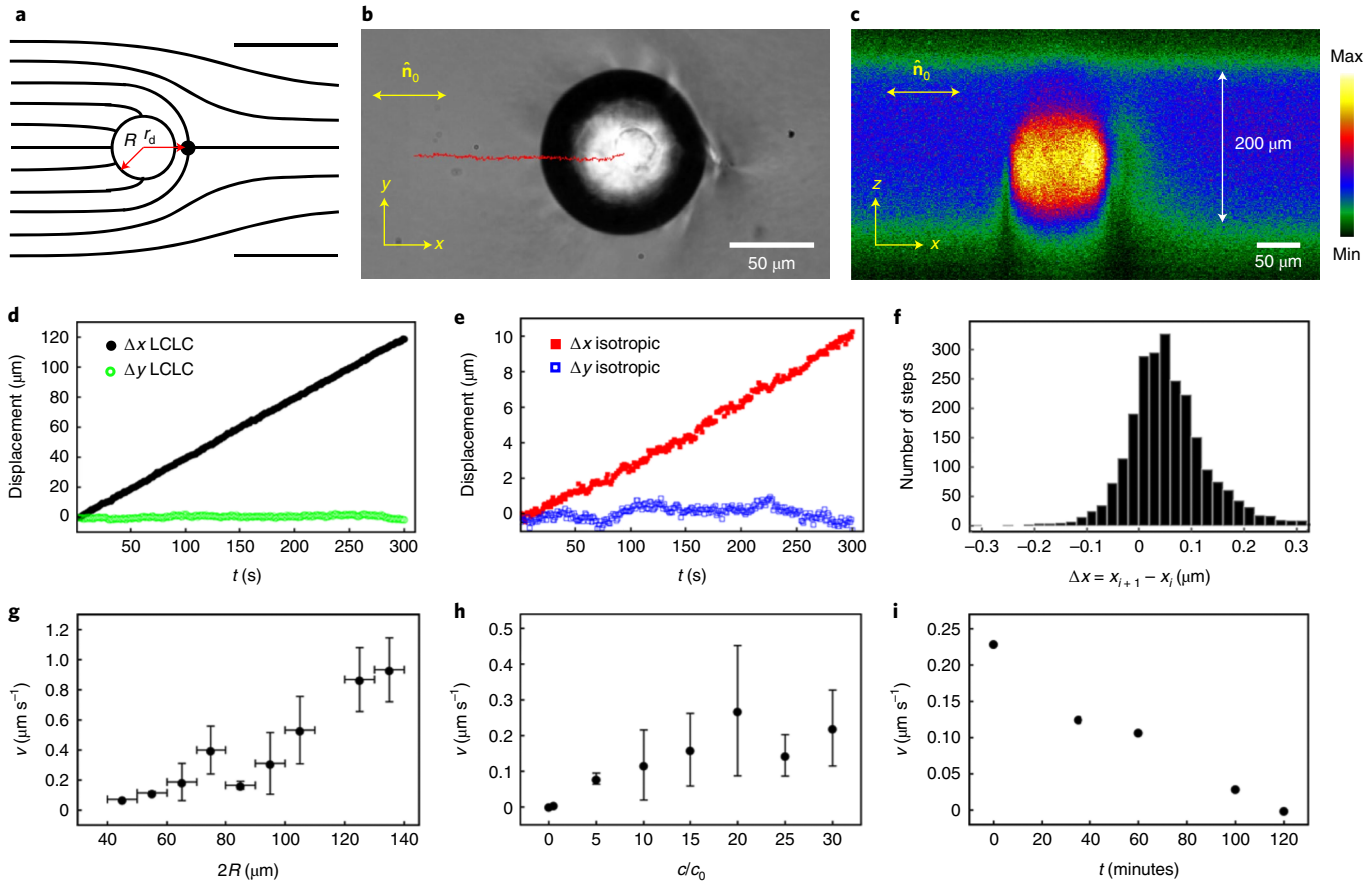

Fig. 1 | Self-propelled active HH droplets. a, Director configuration around a sphere with perpendicular surface anchoring that produces a point-defect HH. **b**, Optical microscopy texture (no polarizers) of a self-propelled droplet; the red trajectory is traced for 10 min. **c**, Fluorescent confocal polarizing microscopy texture of the vertical cross-section of a sample with the LCLC-based active droplet in the middle; colour corresponds to the intensity of the fluorescent signal from the sample. **d**, Displacements Δx along $\hat{\mathbf{n}}_0$ and Δy in the perpendicular direction, measured every 1 s for LCLC-based active droplet, $2R = 90\,\mu m$, $c = 20c_0$. **e**, The same for an isotropic active droplet with $2R = 90\,\mu m$, $c = 20c_0$. **f**, Histogram of droplet displacements measured within 0.05 s intervals along the x axis, positive steps are towards the hedgehog; $2R = 135\,\mu m$, $c = 20c_0$. **g**, Propulsion speed v versus droplet diameter $2R$, $c = 20c_0$. **h**, v versus bacterial concentration, $2R = (90 \pm 5)\,\mu m$. **i**, Slowing down of a single droplet in which the bacteria stop to swim after about 2 h; $2R = 120\,\mu m$, $c = 5c_0$. All data, except for **i**, are obtained within 30 min since sample preparation. Error bars represent standard deviation; the plots in **h** and **g** were constructed by tracking 200 drops, with 10 being the typical number of drops corresponding to each point with a fixed set of parameters.

range $r_d = (1.2 \pm 0.1)R$, which is wider than $r_d = (1.18 \pm 0.05)R$ measured for inactive drops. Angular fluctuations of $\mathbf{r}_d$ are $\pm(10–15)°$, similar to the case of an inactive sphere moved by gravity[27], but much larger than $\pm 1°$ expected for an equilibrium HH structure[28]. The enhancement of $\mathbf{r}_d$ fluctuations should be attributed to the active flows transferred through the interface.

The self-produced locomotion is not strictly unidirectional, when observed within short time intervals such as 0.05 s in Fig. 1f: the droplet makes steps forward and backward along the x axis, but the motion towards the hedgehog prevails (Fig. 1d–f). Shifts along the y axis perpendicular to $\hat{\mathbf{n}}_0$ are random and produce no net displacement over time (Fig. 1d,e). The speed of active droplets along $\hat{\mathbf{n}}_0$ depends on the composition: LCLC-based droplets move about ten times faster than their isotropic counterparts. For example, an isotropic droplet with $2R = 90\,\mu m$ and $c = 20c_0$ moves with $v \approx 2\,\mu m\,min^{-1}$ (Fig. 1e), while a similar LCLC droplet shows $v \approx 24\,\mu m\,min^{-1}$ (Fig. 1d). The propulsion speed increases with the droplet's diameter (Fig. 1g) and with the concentration of bacteria (Fig. 1h). As time goes by and the bacteria consume nutrients and oxygen, their activity diminishes, and v decreases, as illustrated for one such drop in Fig. 1i. Droplets without bacteria show no locomotion.

The SR configuration around active droplets is of a quadrupolar symmetry (Fig. 2a,b) and yields no rectified propulsion. The SR droplets show anisotropic diffusion[29,30]; with the displacements along $\hat{\mathbf{n}}_0$ longer than in the perpendicular direction (Fig. 2c,d). The SRs fluctuate, being perturbed by active flows inside the droplets, similarly to SRs around active nematic spherical shells[31]. The fluctuations shift the SR from the equatorial location, which we quantify by the ratio r_d/R, where r_d is the distance from the drop's centre to the plane of the ring (Fig. 2f). Left and right shifts are of equal probability. Once the SR shifts, the director field becomes polar and the droplet starts to move along the direction of shift, with $v \propto r_d/R$ (Fig. 2e,f). If the SR returns to the equatorial location, the droplet stops. The same droplet can move to the right and left, following the direction of the SR shift (Fig. 2f and Supplementary Video 2). The highest speed is achieved when the SR shrinks into the hedgehog, thus maximizing $|r_d/R|$ (Fig. 2e,g). Although a hedgehog can expand into an SR, say, by applying an electric field[32,33], we do not observe a full reversal of an HH back into an equatorial SR.

The shift of the SR towards the front of the moving droplet in Fig. 2 is opposite to the SR shift downstream observed for passive isotropic droplets moved through a thermotropic nematic by gravity[34]. Another interesting observation is that in the case of an SR (Fig. 2),

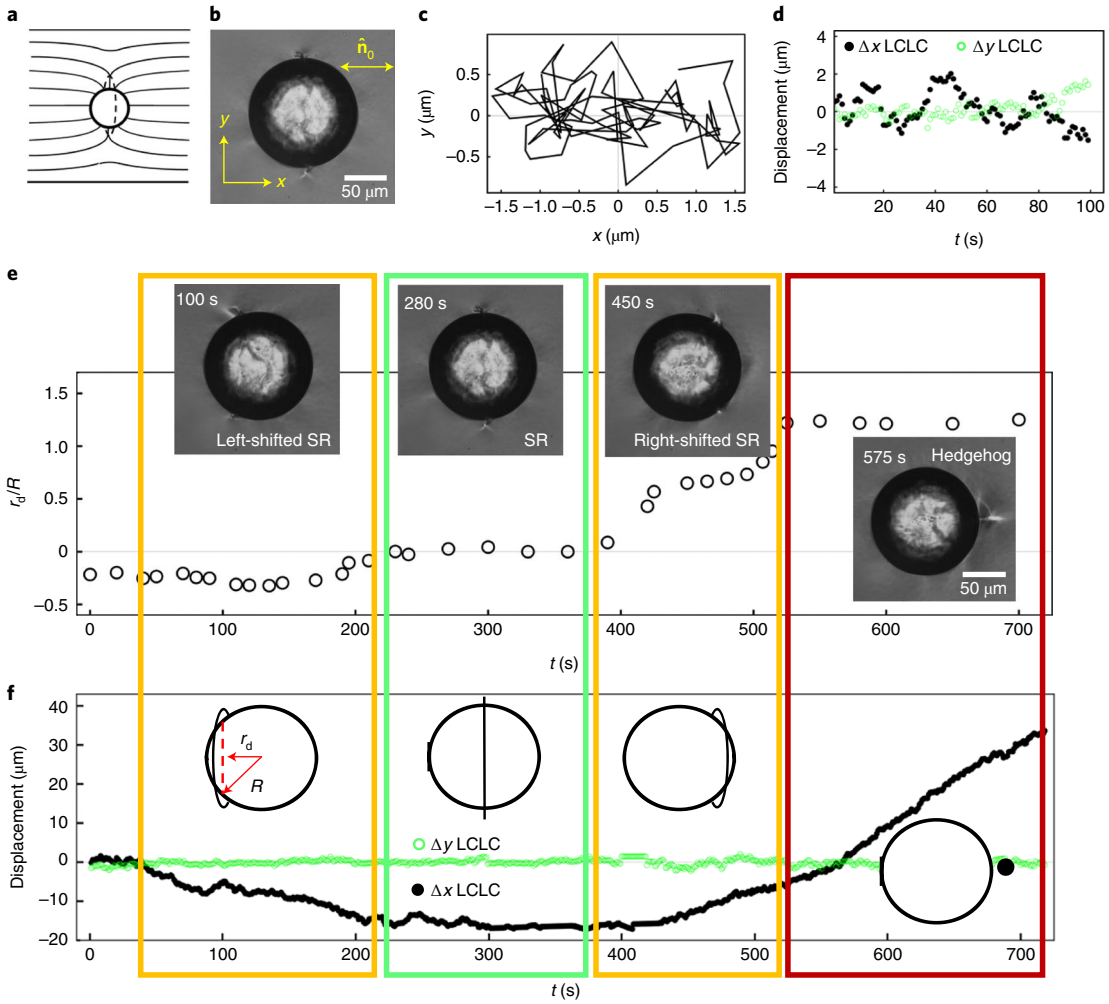

Fig. 2 | Active droplet accompanied by an SR. a, SR director configuration around a sphere with perpendicular surface anchoring. **b**, Optical microscopy texture (no polarizers) of an SR droplet of quadrupolar symmetry. **c**, The trajectory of the SR droplet traced during 100 s; no net displacement. **d**, Displacements Δx along $\hat{\mathbf{n}}_0$ and Δy in a perpendicular direction, measured every 1 s. **e**, The SR around the droplet is strongly shifted by active flows, first to the left ($t<220$ s), then back to the equatorial position ($220\,\text{s}<t<370\,\text{s}$), then to the right ($370\,\text{s}<t<520\,\text{s}$); the SR eventually shrinks into a hedgehog ($t>520$ s); the plot shows the time evolution of the asymmetry degree r_d/R. **f**, (x,y) coordinates of the same active droplet as in **e** within the same time interval; the velocity of self-propulsion grows with the degree of asymmetry $|r_d/R|$. All data are obtained within 30 min since sample preparation for the same LCLC-based droplet with $2R=130\,\mu$m, $c=20c_0$.

the Ericksen number of the overall balance of the viscous drag and elastic forces, $\text{Er}=\eta_N vR/K$, is low: with $2R=130\,\mu$m, average viscosity of the nematic $\eta_N=0.1\,\text{kg m}^{-1}\text{s}^{-1}$, $K\approx10\,\text{pN}$ and $v=0.1\,\mu\text{m s}^{-1}$, one finds $\text{Er}\approx0.1$. Flows at such a low Er should not cause a substantial modification of the director[34–36]. It means that the strong SR shape fluctuations in Fig. 2 are caused by the local turbulent flows with instantaneous velocities $|v_a|$ that are higher than v.

The nematic environment can be pre-aligned in various spatially varying $\hat{\mathbf{n}}_0(x,y)$ patterns[37] to command the droplets to follow a preset path. The effect is illustrated for HH droplets that self-propel along the circular trajectories in Fig. 3 and Supplementary Video 3. The HH droplets in both unidirectional and circular cells can interact. For example, droplets of the same polarity can form linear chains and move entrained. These interactions will be presented in a separate study.

Self-locomotion is pertinent to only an active droplet that develops a director structure of polar symmetry around it. The HH structures are the fastest, while the SR droplets of quadrupolar symmetry are not motile but become mobile when the SR shifts from the equatorial position and the director field becomes polar. The polar director field rectifies the random flows of the bacterial swimmers inside the droplets into the directional flows outside the droplet and enables long-range unidirectional propulsion.

Particle image velocimetry (PIV) of fluorescent tracers reveals chaotic interior flows at the explored concentrations $c\geq4\times10^{15}\,\text{m}^{-3}$, with vortices that are poorly correlated in space and time (Fig. 4a,b and Supplementary Video 4). The maps of interior velocity $\mathbf{v}_{in}$ and colour-coded vorticity $\omega=\partial v_{in,y}/\partial x-\partial v_{in,x}/\partial y$ show no spatial correlations above distances $L_{corr}=30$–$40\,\mu$m and times $t\approx2$–3 s (Fig. 4a). The interior velocities increase near the droplet surface (Fig. 4a–c and Supplementary Video 4). The root-mean-square value $|v_{in,\varphi}|$ of the azimuthal velocity is approaching the root mean square of the overall speed $|v_{in}|$ near the droplet surface, indicating that the flows are predominantly tangential to the spherical interface (Fig. 4c). There is no preferred direction of circulation, since the azimuthal component $v_{in,\varphi}$, averaged over a circle of a constant radius $r<R$ is much smaller than $|v_{in,\varphi}|$ (Fig. 4c). This behaviour is different from steady counter-rotating circulations known for quasi-two-dimensional droplets[38]. An apparent reason is that the bacterial activity is distributed uniformly within the subsurface

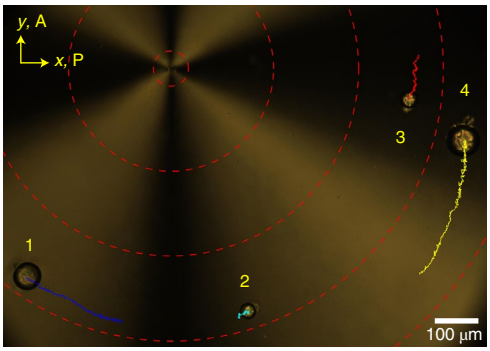

Fig. 3 | Circular trajectories of active HH droplets in a nematic with a circular prepatterned director. (1) Droplet of diameter $2R = 68\,\mu m$, speed $v = 0.11\,\mu m\,s^{-1}$, moving along a circular trajectory at a radial distance 640 μm from the pattern's centre; (2) $2R = 40\,\mu m$, $v = 0.01\,\mu m\,s^{-1}$, distance 634 μm; (3) $2R = 50\,\mu m$, $v = 0.06\,\mu m\,s^{-1}$, distance 606 μm; (4) $2R = 85\,\mu m$, $v = 0.14\,\mu m\,s^{-1}$, distance 750 μm. The dashed lines show the prepatterned director. The data are obtained for LCLC-based droplets with bacterial concentration $c = 5c_0$, within 40 min since sample preparation. Polarizing optical microscopy with crossed polarizers A and P.

region, showing no anomalies underneath the HH and SR defects. This homogenization is supported by the spherical geometry, which also introduces singularities in the velocity field because of the Euler–Poincaré theorem[20].

The active flows transferred through the interface cause director realignment and flows of the nematic (Fig. 4d and Supplementary Videos 1 and 2). The swimming bacteria do not perturb much the interfacial area. As pointed out by Ramos et al.[14], the surface tension $\sigma \approx 10^{-3}\,J\,m^{-2}$ of a water–oil interface such as explored in our work makes deformations by swimming bacteria unlikely. An excess area l^2, where l is the bacterium size, requires an increase of the surface energy $\sim\sigma l^2$. A bacterium, swimming over the same length l, performs a work roughly equivalent to $fl \approx \eta_{LCLC} l^2 v_B$, where $f \approx \eta_{LCLC} l v_B$ is the thrust force of a bacterium, $v_B \approx 10\,\mu m\,s^{-1}$ is its speed and $\eta_{LCLC} \approx 0.1\,kg\,m^{-1}\,s^{-1}$ is the viscosity of the studied LCLC[39]. Since $\sigma/(\eta_{LCLC} v_B) \approx 10^3$ the surface tension prevails. In contrast, the anisotropic part of the surface tension, $W \approx 10^{-6}\,J\,m^{-2}$, estimated above, is much weaker than σ, so that $W/(\eta_{LCLC} v_B) \approx 1$. The last feature explains the director realignments outside the droplet caused by the active shears in the interior. Similar director realignment of a thermotropic nematic in contact with a bacterial aqueous bath was observed by Kim et al[40].

The exterior flows extend over hundreds of micrometres (Fig. 4d–f). Unlike the interior flows, they yield a net flow, rectified by the polar HH structure (Fig. 4d–f). In the droplet's coordinate system, the nematic flows from the hedgehog towards the droplet (Fig. 4d). In the laboratory system, it means that the active droplet self-propels with the hedgehog (or the shifted SR) leading the way (Supplementary Videos 1 and 2). The rectification is rooted in the well-known flow–director coupling that causes a non-Newtonian behaviour and the so-called backflow, that is, flow induced by director reorientations[20]. The director relaxation time is relatively long, compared with the correlation times inside the droplet (Fig. 4a): $t_N \approx \eta_N R^2/K > 10\,s$ for the thermotropic nematic viscosity $\eta_N = 0.1\,kg\,m^{-1}\,s^{-1}$ and $R > 30\,\mu m$, which means that the activity-perturbed director is persistently out of equilibrium, rotating and causing nematic backflows. An important feature of the non-equilibrium director–flow coupling is that the torque equation in the Ericksen–Leslie theory is not invariant under reversals of local velocities, $\mathbf{v}(\mathbf{r},t) \to -\mathbf{v}(\mathbf{r},t)$ (Supplementary Information). Stark and Ventzki[32] presented a particularly clear illustration: the Stokes drag on a sphere with an HH structure depends on whether the flow is towards the sphere or the hedgehog. Another example is directional pumping in the so-called hybrid-aligned nematic cell[41]. A plate that aligns $\hat{\mathbf{n}}$ perpendicularly to itself moves periodically right (+) and left (−) with respect to an immobile plate that aligns $\hat{\mathbf{n}}$ parallel to the shifts[41]. Although the shifts are not biased, simulations by Zhang et al.[41] revealed a directional volumetric flow rate Φ of the nematic, $\Delta\Phi/\Phi_0 = (|\Phi_-| - |\Phi_+|)/\Phi_0 \neq 0$, where Φ_0 is the flow rate of a Newtonian fluid under the same shear rate. The pumping direction depends on the rotation sense of the director from the bottom to the top plate[42] and on Er[41]. Defining Er through the instantaneous tangential speed $v_a \approx (0.1\text{–}10)\,\mu m\,s^{-1}$ of the interior velocities that are transmitted into the nematic, one finds $Er = \eta_N v_a R/K \approx 0.1\text{–}10$. The simulations[41] show that rectification of the flow is most effective at these values of Er, achieving $\Delta\Phi/\Phi_0 \approx \pm 0.1$. Although the geometry of the one-dimensionally distorted hybrid-aligned nematic is relatively simple, the emerging backflow behaviour is so complex that asymmetric flows and quantities such as $\Delta\Phi$ could be found only numerically[32,41,42]; an analytic description is prohibitively difficult.

The flow rectification by polar director deformations around active droplets is similar to that in refs. [32,41,42]. Consider, for example, the regions above and below a droplet (Fig. 4g) where the director is hybrid-aligned. In the absence of flows, $\hat{\mathbf{n}}$ rotates by 90° from a normal to the droplet's surface to $\hat{\mathbf{n}}_0 = (1, 0, 0)$, as one moves away by some distance $\geq R$. The location of the hedgehog fixes the sense of rotation. If the hedgehog is on the right (Fig. 4g), $\hat{\mathbf{n}}$ rotates counterclockwise (CCW) above the droplet and clockwise (CW) below it. When the bacteria cause tangential flows and vorticity at the interface, these transfer into the nematic. As follows from the experiments (Fig. 4a), the bacterial flows are not biased: velocity of right and left flows along the interface in Fig. 4g averaged over times longer than a few seconds are of the same amplitude, $\langle |v_{a,+}| \rangle = \langle |v_{a,-}| \rangle = \langle |v_a| \rangle$. Although unbiased, these flows trigger a polar viscous response in the nematic. For example, below the droplet, a right impulse $\propto v_{a,+}$ imposes a CW torque on the CW-rotated $\hat{\mathbf{n}}$, while a left impulse $\propto v_{a,-}$ means a CCW torque on the same CW-rotated $\hat{\mathbf{n}}$ (Fig. 4g). These two different combinations of the torque polarity and director rotation produce different out-of-equilibrium director $\hat{\mathbf{n}}_+(\mathbf{r},t) \neq \hat{\mathbf{n}}_-(\mathbf{r},t)$ (refs. [41,42]) and thus different viscosities $\eta_+ \neq \eta_-$ (Fig. 4g), as the viscosity depends on the director configuration. Mirror symmetry of the top and bottom regions of the sample with respect to the horizontal xy plane ensures the same polarity of the rectified flows in these regions, as observed (Fig. 4e).

The difference $\eta_+ \neq \eta_-$ yields a rectified propulsion force that can be estimated roughly as $F_a \approx CR\langle |v_a| \rangle (\eta_+ - \eta_-)$, where C is a numerical factor that depends on the slip conditions. Since the hedgehog leads the way (Fig. 1b and Supplementary Videos 1 and 2), $\mathbf{F}_a$ is directed from the sphere towards the hedgehog. As self-locomotion is force free, F_a should be balanced by the Stokes drag that can be estimated as $F_{drag} = C\eta_N R v$, where $\eta_N \approx 0.1\,kg\,m^{-1}\,s^{-1}$ is the average viscosity of the nematic, which yields an estimate for the self-propulsion speed $v \approx \langle |v_a| \rangle (\eta_+ - \eta_-)/\eta_N$. With $\langle |v_a| \rangle \approx 1\text{–}10\,\mu m\ s^{-1}$ and $v \approx 0.1\text{–}1\,\mu m\,s^{-1}$, the required viscous anisotropy is modest, $(\eta_+ - \eta_-)/\eta_N \approx 0.01 - 1$, which is well within reach for thermotropic nematics[20,41]. Similar estimates can be obtained by considering the differences in the director field near the hedgehog and at the opposite pole of the droplet, where the director is close to uniform.

Propulsion of a sphere with an SR shifted from the equatorial location is explained similarly by the acquired polar character of the director field, which sets $\eta_+ \neq \eta_-$ and rectifies directional flows around the sphere. When the SR shifts to the right, the director structure above and below the droplet becomes similar to the pattern in Fig. 4g.

As already indicated, the dynamics is accompanied by a small fraction of backward displacements, when tracking is within a short time interval, such as 0.05 s in Fig. 1f. The phenomenon is not

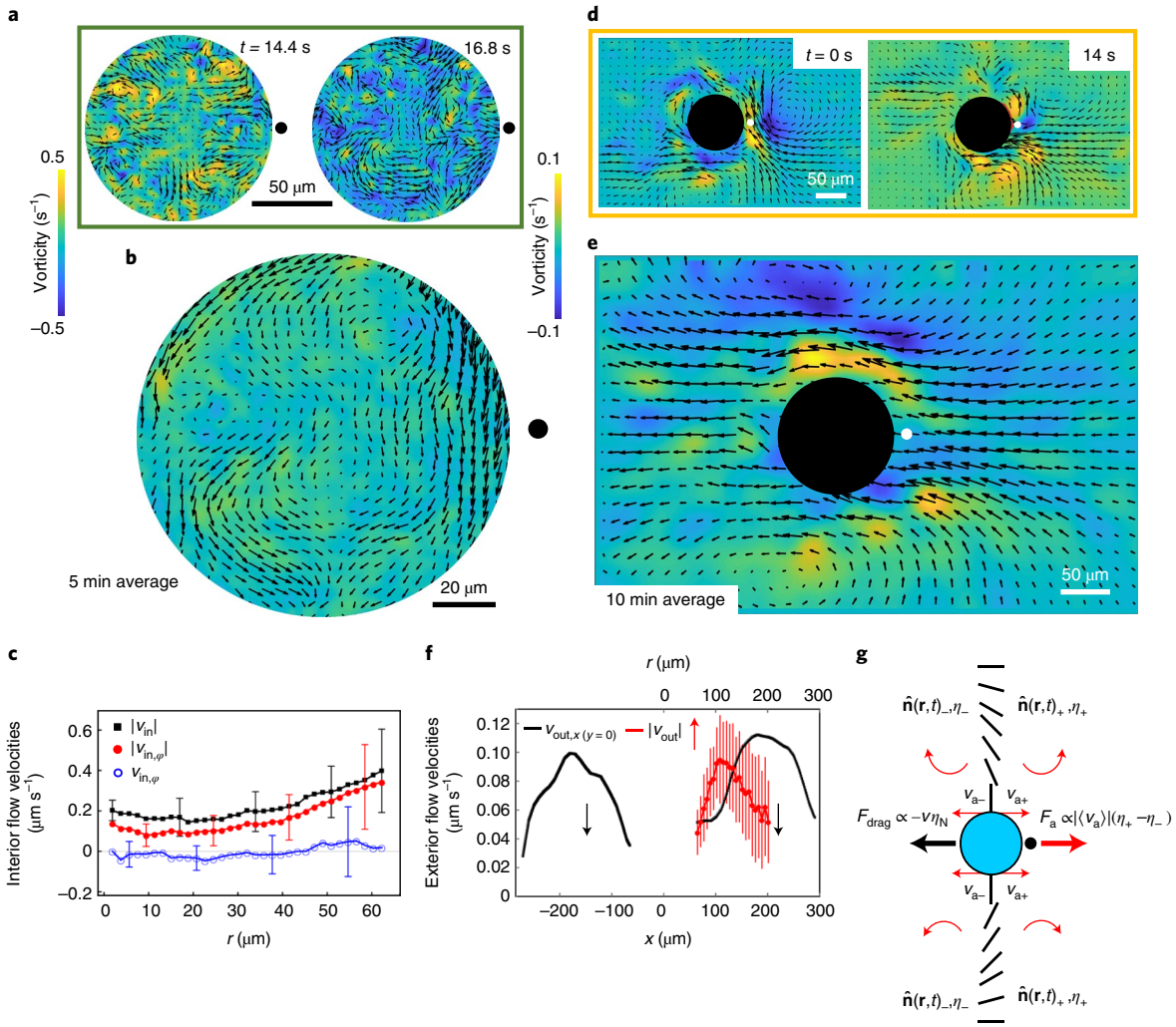

Fig. 4 | Activity triggered flows inside and outside the HH droplet. a, Two maps of instantaneous velocity (maximum 6 μm s^{-1}) and colour-coded vorticity of active flows in an active droplet with $2R = 125$ μm, $c = 20c_0$, documented within 2.4 s of each other. **b**, The same droplet, velocity and vorticity are averaged over 5 min; maximum velocity 1 μm s^{-1}. **c**, The root-mean-square interior velocity $|v_{in}|$, azimuthal component $v_{in,\varphi}$, and its root-mean-square value $|v_{in,\varphi}|$ versus the distance $r < R$ from the droplet centre, calculated using data in part **b**. The error bars represent s.d. **d**, Velocity (maximum 2 μm s^{-1}) and vorticity of nematic flows outside an active droplet with $2R = 110$ μm, $c = 20c_0$. **e**, The same droplet, velocity (maximum 0.2 μm s^{-1}) and vorticity are averaged over 10 min. The black arrows in panels **a**,**b**,**d**, and **e** indicate the local flow velocity; their length is proportional to the local speed. **f**, The root mean square of the outside flow velocity calculated as a function of $r > R$ and the x component of velocity along the x axis centred at the droplet centre, calculated using the data in **e**. All data in **a**–**f** are obtained for LCLC-based droplets within 30 min since sample preparation. **g**, Self-propulsion mechanism of a droplet with a hedgehog (black disk) on its right-hand side. Bacterial-activity-created velocities directed to the right, $\mathbf{v}_{a+}$, and to the left, $\mathbf{v}_{a-}$, perturb the hybrid-aligned director above (and below) the droplet differently, yielding two different director fields $\hat{\mathbf{n}}(\mathbf{r},t)_+ \neq \hat{\mathbf{n}}(\mathbf{r},t)_-$ and two viscous resistances $\eta_+ \neq \eta_-$, which result in the rectified active force F_a. Red colour denotes vector quantities brought about by bacterial activity. The core of the hedgehog is shown as a small black sphere in panels **a**,**b** and **g**, and as a white sphere in panels **d** and **e**. The large black sphere in panels **d** and **e** shows the active droplet.

surprising given the bacterial turbulence in the interior, in which the net active shear stresses can point in any direction at a given instance of time. One might wonder whether droplets of the size of vortices, 30–40 μm or smaller, could show coherent flows. The answer is negative, we do not see any coherent motion in smaller droplets. While the increase of the droplet speed v with the concentration of bacteria is intuitively clear because of the increased activity, a higher v in the nematic LCLC as opposed to the aqueous dispersion is less obvious but correlates with the previous findings. First, the effective viscosity $\eta_{LCLC} = 0.1\,\mathrm{kg\,m^{-1}\,s^{-1}}$ of the LCLC is higher than the viscosity of water, which helps in the momentum transfer through the droplet–nematic interface. Second, despite this viscosity increase, the speed of *B. subtilis* in the LCLC is only ~25% lower than that in water[43]. Third, the LCLC enhances the turbulence flows rather than suppresses them, causing turbulence with disclinations already at $c \approx 10^{14}\,\mathrm{m^{-3}}$ (ref. [26]), which is ten times lower than the concentrations triggering turbulence in water[24].

The propulsive ability of the active droplets cannot be explained by the Marangoni effect associated with a dynamic redistribution of lecithin and gradients of the interfacial tension, as droplets with the surfactant but no active bacteria show no rectified motility, even when the concentration of lecithin is increased to 1 wt%. Droplets smaller than 30 μm do not show rectified flows and thus do not exhibit self-locomotion (Fig. 1g), apparently because the number of bacteria is not sufficient to produce strong flows. Another factor diminishing the self-locomotion ability of small droplets might be the steeper decrease of surface anchoring energy ($\sim WR^2$) compared with bulk elasticity of the nematic ($\sim KR$).

Conclusion

We demonstrated an approach to extract work from random motion of microswimmers and to power rectilinear and curvilinear self-locomotion of active droplets. The concrete example is based on swimming bacteria, dispersed in aqueous media with nutrients and with or without additional ingredients such as the LCLC. These dispersions are emulsified as active droplets in a thermotropic nematic with an added surfactant that produces a locally radial orientation of the nematic director around the droplet. The local radial director matches the uniform far field through topological defects, either a hyperbolic hedgehog on one side or an equatorial 'Saturn ring' of a disclination loop. When the active droplet develops a fore-aft asymmetric director structure, either with a hedgehog or with a shrunk Saturn ring, it acquires the ability to propel itself along a rectilinear or curvilinear trajectory that is set by the overall director of the thermotropic nematic environment.

The active flows generated by bacteria inside the droplet trigger flows in the nematic that are rectified by the polar director structure into a net directional flow. The efficiency of self-propulsion is directly related to the degree of polar asymmetry, as shown by the shifted SR in Fig. 2 and Supplementary Video 2. The droplets formed by dispersions of bacteria in LCLCs show a faster speed than their isotropic counterparts (Fig. 1d,e). The droplets with hedgehogs move faster when they are larger and when the concentration of bacteria is higher. Droplets without motile bacteria or with bacteria that stopped swimming do not propel. By patterning the overall director field of the environment, one can predesign the geometry of trajectories.

The demonstrated mechanism adds to the set of principles of microscale swimming described by Purcell[15] for isotropic Newtonian fluids, in which the simplest swimmers are either three identical spheres connected by slender rods of changing length[44] or two connected spheres exchanging material between themselves[45]. In the nematic environment, owing to orientational order and associated surface anchoring and elasticity, the simplest swimmer is a single sphere that produces a satellite topological defect in its neighbourhood. It acquires mobility through rectification of the chaotic internal motion by the asymmetric molecular orientation pattern of the environment. The dependency of self-propulsion speed $v \approx \langle |v_a| \rangle (\eta_+ - \eta_-)/\eta_N$ on the difference in the viscous coefficients underscores the non-Newtonian and anisotropic nature of the propulsion mechanism.

The rectilinear and curvilinear self-locomotion of active droplets enabled by a liquid-crystal environment could find applications in the future development of micromachines. The principle should be extendable to other systems, for example, synthetic microswimmers. The described phenomenon adds to the growing list of physical effects enabled by liquid crystals used instead of isotropic fluids as a medium for dynamics[33,40,46,47]. Recent theoretical works on swimming in a nematic[48–51], although not addressing the geometry proposed in this work, suggest that the liquid-crystal environment offers a broad range of possibilities to control microscale dynamics, by means such as surface anchoring[48] and director coupling to the propulsion mechanism[49,50]. It would be of interest to explore these opportunities, by varying many parameters offered by the described system.

Online content

Any methods, additional references, Nature Research reporting summaries, source data, extended data, supplementary information, acknowledgements, peer review information; details of author contributions and competing interests; and statements of data and code availability are available at https://doi.org/10.1038/s41567-020-01055-5.

Received: 27 March 2020; Accepted: 27 August 2020;
Published online: 12 October 2020

References

1. Joanny, J. F. & Ramaswamy, S. A drop of active matter. *J. Fluid Mech.* **705**, 46–57 (2012).
2. Sanchez, T., Chen, D. T. N., DeCamp, S. J., Heymann, M. & Dogic, Z. Spontaneous motion in hierarchically assembled active matter. *Nature* **491**, 431–434 (2012).
3. Vladescu, I. D. et al. Filling an emulsion drop with motile bacteria. *Phys. Rev. Lett.* **113**, 268101 (2014).
4. Giomi, L. & DeSimone, A. Spontaneous division and motility in active nematic droplets. *Phys. Rev. Lett.* **112**, 147802 (2014).
5. Khoromskaia, D. & Alexander, G. P. Motility of active fluid drops on surfaces. *Phys. Rev. E* **92**, 062311 (2015).
6. Zwicker, D., Seyboldt, R., Weber, C. A., Hyman, A. A. & Julicher, F. Growth and division of active droplets provides a model for protocells. *Nat. Phys.* **13**, 408–413 (2017).
7. Loisy, A., Eggers, J. & Liverpool, T. B. Tractionless self-propulsion of active drops. *Phys. Rev. Lett.* **123**, 248006 (2019).
8. Weirich, K. L., Dasbiswas, K., Witten, T. A., Vaikuntanathan, S. & Gardel, M. L. Self-organizing motors divide active liquid droplets. *Proc. Natl Acad. Sci. USA* **116**, 11125–11130 (2019).
9. Kruger, C., Klos, G., Bahr, C. & Maass, C. C. Curling liquid crystal microswimmers: a cascade of spontaneous symmetry breaking. *Phys. Rev. Lett.* **117**, 048003 (2016).
10. Cates, M. E. & Tjhung, E. Theories of binary fluid mixtures: from phase-separation kinetics to active emulsions. *J. Fluid Mech.* **836**, P1 (2017).
11. Gao, T. & Li, Z. R. Self-driven droplet powered by active nematics. *Phys. Rev. Lett.* **119**, 108002 (2017).
12. Copar, S., Aplinc, J., Kos, Z., Zumer, S. & Ravnik, M. Topology of three-dimensional active nematic turbulence confined to droplets. *Phys. Rev. X* **9**, 031051 (2019).
13. Morozov, M. & Michelin, S. Orientational instability and spontaneous rotation of active nematic droplets. *Soft Matter* **15**, 7814–7822 (2019).
14. Ramos, G., Cordero, M. L. & Soto, R. Bacteria driving droplets. *Soft Matter* **16**, 1359–1365 (2020).
15. Purcell, E. M. Life at low Reynolds-number. *Am. J. Phys.* **45**, 3–11 (1977).
16. Howse, J. R. et al. Self-motile colloidal particles: from directed propulsion to random walk. *Phys. Rev. Lett.* **99**, 048102 (2007).
17. Marchetti, M. C. Spontaneous flows and self-propelled drops. *Nature* **491**, 340–341 (2012).
18. Sokolov, A., Apodaca, M. M., Grzybowski, B. A. & Aranson, I. S. Swimming bacteria power microscopic gears. *Proc. Natl Acad. Sci. USA* **107**, 969–974 (2010).
19. Di Leonardo, R. et al. Bacterial ratchet motors. *Proc. Natl Acad. Sci. USA* **107**, 9541–9545 (2010).
20. Kleman, M. & Lavrentovich, O. D. *Soft Matter Physics: An Introduction* (Springer, 2003).
21. Poulin, P., Stark, H., Lubensky, T. C. & Weitz, D. A. Novel colloidal interactions in anisotropic fluids. *Science* **275**, 1770–1773 (1997).
22. Kuksenok, O. V., Ruhwandl, R. W., Shiyanovskii, S. V. & Terentjev, E. M. Director structure around a colloid particle suspended in a nematic liquid crystal. *Phys. Rev. E* **54**, 5198–5203 (1996).
23. Gu, Y. D. & Abbott, N. L. Observation of Saturn-ring defects around solid microspheres in nematic liquid crystals. *Phys. Rev. Lett.* **85**, 4719–4722 (2000).
24. Dombrowski, C., Cisneros, L., Chatkaew, S., Goldstein, R. E. & Kessler, J. O. Self-concentration and large-scale coherence in bacterial dynamics. *Phys. Rev. Lett.* **93**, 098103 (2004).
25. Sokolov, A. & Aranson, I. S. Physical properties of collective motion in suspensions of bacteria. *Phys. Rev. Lett.* **109**, 248109 (2012).
26. Zhou, S., Sokolov, A., Lavrentovich, O. D. & Aranson, I. S. Living liquid crystals. *Proc. Natl Acad. Sci. USA* **111**, 1265–1270 (2014).
27. Pages, J. M., Ignes-Mullol, J. & Sagues, F. Anomalous diffusion of motile colloids dispersed in liquid crystals. *Phys. Rev. Lett.* **122**, 198001 (2019).
28. Lubensky, T. C., Pettey, D., Currier, N. & Stark, H. Topological defects and interactions in nematic emulsions. *Phys. Rev. E* **57**, 610–625 (1998).
29. Loudet, J. C., Hanusse, P. & Poulin, P. Stokes drag on a sphere in a nematic liquid crystal. *Science* **306**, 1525–1525 (2004).
30. Turiv, T. et al. Effect of collective molecular reorientations on brownian motion of colloids in nematic liquid crystal. *Science* **342**, 1351–1354 (2013).
31. Hardouin, J., Guillamat, P., Sagues, F. & Ignes-Mullol, J. Dynamics of ring disclinations driven by active nematic shells. *Front. Phys.* **7**, 165 (2019).
32. Stark, H. & Ventzki, D. Non-linear Stokes drag of spherical particles in a nematic solvent. *Europhys. Lett.* **57**, 60–66 (2002).
33. Lavrentovich, O. D. Active colloids in liquid crystals. *Curr. Opin. Colloid* **21**, 97–109 (2016).
34. Khullar, S., Zhou, C. F. & Feng, J. J. Dynamic evolution of topological defects around drops and bubbles rising in a nematic liquid crystal. *Phys. Rev. Lett.* **99**, 237802 (2007).
35. Fukuda, J., Stark, H., Yoneya, M. & Yokoyama, H. Dynamics of a nematic liquid crystal around a spherical particle. *J. Phys. Condens. Mat.* **16**, S1957–S1968 (2004).

36. Zhou, C., Yue, P. & Feng, J. J. The rise of Newtonian drops in a nematic liquid crystal. *J. Fluid Mech.* **593**, 385–404 (2007).
37. Guo, Y. et al. High-resolution and high-throughput plasmonic photopatterning of complex molecular orientations in liquid crystals. *Adv. Mater.* **28**, 2353–2358 (2016).
38. Wioland, H., Woodhouse, F. G., Dunkel, J., Kessler, J. O. & Goldstein, R. E. Confinement stabilizes a bacterial suspension into a spiral vortex. *Phys. Rev. Lett.* **110**, 268102 (2013).
39. Habibi, A., Blanc, C., Ben Mbarek, N. & Soltani, T. Passive and active microrheology of a lyotropic chromonic nematic liquid crystal disodium cromoglycate. *J. Mol. Liq.* **288**, 111027 (2019).
40. Kim, Y. K., Noh, J., Nayani, K. & Abbott, N. L. Soft matter from liquid crystals. *Soft Matter* **15**, 6913–6929 (2019).
41. Zhang, R., Roberts, T., Aranson, I. S. & de Pablo, J. J. Lattice Boltzmann simulation of asymmetric flow in nematic liquid crystals with finite anchoring. *J. Chem. Phys.* **144**, 084905 (2016).
42. Marenduzzo, D., Orlandini, E. & Yeomans, J. M. Interplay between shear flow and elastic deformations in liquid crystals. *J. Chem. Phys.* **121**, 582–591 (2004).
43. Sokolov, A., Zhou, S., Lavrentovich, O. D. & Aranson, I. S. Individual behavior and pairwise interactions between microswimmers in anisotropic liquid. *Phys. Rev. E* **91**, 013009 (2015).
44. Najafi, A. & Golestanian, R. Simple swimmer at low Reynolds number: three linked spheres. *Phys. Rev. E* **69**, 062901 (2004).
45. Avron, J. E., Kenneth, O. & Oaknin, D. H. Pushmepullyou: an efficient micro-swimmer. *N. J. Phys.* **7**, 234 (2005).
46. Lavrentovich, O. D. Transport of particles in liquid crystals. *Soft Matter* **10**, 1264–1283 (2014).
47. Sokolov, A., Mozaffari, A., Zhang, R., de Pablo, J. J. & Snezhko, A. Emergence of radial tree of bend stripes in active nematics. *Phys. Rev. X* **9**, 031014 (2019).
48. Shi, J. & Powers, T. R. Swimming in an anisotropic fluid: how speed depends on alignment angle. *Phys. Rev. Fluids* **2**, 123102 (2017).
49. Lintuvuori, J. S., Wurger, A. & Stratford, K. Hydrodynamics defines the stable swimming direction of spherical squirmers in a nematic liquid crystal. *Phys. Rev. Lett.* **119**, 068001 (2017).
50. Daddi-Moussa-Ider, A. & Menzel, A. M. Dynamics of a simple model microswimmer in an anisotropic fluid: implications for alignment behavior and active transport in a nematic liquid crystal. *Phys. Rev. Fluids* **3**, 094102 (2018).
51. Kos, Z. & Ravnik, M. Elementary flow field profiles of micro-swimmers in weakly anisotropic nematic fluids: Stokeslet, stresslet, rotlet and source flows. *Fluids* **3**, 15 (2018).

Methods

Active droplets. We use *B. subtilis* strain 1085, which is a rod-shaped bacterium 5–7 μm long and ~0.7 μm in diameter. The bacteria are initially grown on Lysogeny broth (Miller composition from Teknova) agar plates at 35 °C for 12–24 h, then a colony is transferred to a TB liquid medium and grown in shaking incubator at temperature 35 °C for 7–9 h. Sealed vials are used to grow the bacteria to increase resistance to oxygen starvation. The bacteria concentration in the growth medium was monitored by measuring the optical density. The bacteria are removed from the incubator at the end of their exponential growth stage, at the concentration $c_0 = 0.8 \times 10^{15}$ cell m^{-3}, and extracted from the liquid medium by centrifugation.

Two types of active droplets are prepared. One is based on an isotropic aqueous TB (Sigma Aldrich) as a dispersion medium. The second medium for bacteria is a nematic LCLC, 13 wt% dispersion of DSCG (Alfa Aesar) in TB. The mixture is a nematic up to 28.5 °C, above which it transitions into a nematic–isotropic coexistence[52]. At room temperature, the effective viscosity of the 13 wt% DSCG LCLC measured for micrometre-size beads diffusing along the director is $\eta_{LCLC} = 0.1$ kg m^{-1} s^{-1} (ref. [39]). The nematic LCLC phase exists in a relatively narrow range of concentrations from 12 wt% to 16 wt%, above which it transforms into a columnar phase. This LCLC is non-toxic to microorganisms[53]. Both isotropic and LCLC-based active droplets are doped with a very small amount (≤0.05 wt%) of egg-yolk lecithin (Sigma Aldrich), which sets a perpendicular orientation of the thermotropic nematic director at the interface.

Inactive thermotropic nematic environment. The bacteria-containing active aqueous dispersions are mixed with a thermotropic nematic in volume proportion 1:50 and vortexed to achieve the emulsion. Two thermotropic nematics are used, pentylcyanobiphenyl (5CB) and MAT-03-382 (both purchased from Merck). MAT-03-382 and 5CB have similar rotational viscosities at room temperature, $\eta_N = 0.11$ kg m^{-1} s^{-1} (data from the manufacturer) and 0.14 kg m^{-1} s^{-1} (ref. [54]), respectively. Both viscosities are close to the interior viscosity of the LCLC-based droplets, $\eta_{LCLC} = 0.1$ kg m^{-1} s^{-1}, which helps in the momentum and vorticity transfer across the interface. The two thermotropic nematics used as a passive medium yield similar results, with the droplets speed in MAT-03-382 being approximately two times higher than that in 5CB. In the main text, we describe the results for MAT-03-382 only, since the material shows a birefringence of 0.08 at 589 nm (ref. [55]), lower than that of 5CB (0.19), which facilitates optical microscopy. Our LCLC-based system is an inverted active analogue of the nematic-in-LCLC emulsion, in which the thermotropic nematic droplets are dispersed in an LCLC with an added surfactant[56]. The emulsion in ref. [56] does not contain any swimmers, but nematic droplets can propel owing to the Marangoni effect.

The emulsions of active droplets in the thermotropic nematic are filled into cells of thickness $d = 200$ μm, formed by two parallel glass plates. The plates are coated with polyimide PI2555 (Merck) layers and buffed to achieve a unidirectional planar alignment, $\hat{\mathbf{n}}_0 = (1, 0, 0)$ in Cartesian coordinates. The patterned cells such as the one in Fig. 3 are aligned by the plasmonic metamask photoalignment technique[37].

The surfactant lecithin molecules diffuse to the droplet–nematic interface and impose perpendicular alignment of the nematic director $\hat{\mathbf{n}}$ at the surface of active droplets. The hedgehog can form on either side of the droplet; however, once the position is stochastically chosen, the reversal of the polarity is not observed, as it requires energies orders of magnitude higher than the Boltzmann temperature. The hedgehog cores often attract small isotropic or LCLC droplets, of diameter 4 μm or less, to reduce the core energy[57]. These small droplets are used to track the position of the core in Supplementary Fig. 1.

Microscopy characterization. The location of the droplet along the z axis normal to the bounding plates is determined by fluorescent confocal polarizing microscopy[58]. The nematic is doped with the fluorescent hydrophobic dye *N*,*N*′-bis(2,5-di-*tert*-butylphenyl)-3,4,9,10-perylenedicarboximide (BTBP) at 0.0025 wt%, and the active droplets are doped with a hydrophilic dye acridine orange at 0.006 wt%. The in-plane motion of active droplets is observed under a Nikon TE2000 optical microscope equipped with a camera CMOS (Emergent HS-20000C); the trajectories are tracked using ImageJ software[59]. The flows inside and outside of the droplet are visualized by tracking fluorescent polystyrene Suncoast yellow spheres of diameter 200 nm (Bangs Lab), excitation wavelength 540 nm and emission wavelength 600 nm. These wavelengths are safe for bacteria and do not alter their activity over the time of experiments. The fluorescent spheres are dispersed in either the bacterial dispersion or in the nematic environment and tracked by PIV[60], while the microscope is focused at the equatorial plane of the droplets. PIV determines the flow velocities $\mathbf{v}_{in}$ (Fig. 4a,b) and $\mathbf{v}_{out}$ (Fig. 4d,e) inside and outside the droplets, respectively. The azimuthal component $v_{in,\varphi}$ of velocity in Fig. 4c is calculated in the polar coordinate system (r,φ) centred at the droplet's centre, and averaged over all values of the azimuthal angle φ for a given r = constant, $r < R$. The root-mean-square velocity in Fig. 4c is calculated as $|v_{in}| = \sqrt{\frac{1}{N}\sum_{i=1}^{N} |\mathbf{v}_{in,i}|^2}$, by measuring the local velocity projection $\mathbf{v}_{in,i}$ onto the xy plane at N points along a circle r = constant and then averaging the values over $0 \le \varphi < 2\pi$. The root-mean-square azimuthal component of the interior velocity in Fig. 4c and the root-mean-square outside velocity in Fig. 4f are calculated in a similar way, $|v_{in,\varphi}| = \sqrt{\frac{1}{N}\sum_{i=1}^{N} |v_{in,\varphi,i}|^2}$ and $|v_{out}| = \sqrt{\frac{1}{N}\sum_{i=1}^{N} |\mathbf{v}_{out,i}|^2}$.

Reporting Summary. Further information on research design is available in the Nature Research Reporting Summary linked to this article.

Data availability

Source data for Figs. 1d–i, 2c–f and 4c, f are available with this paper. All other data that support the plots within this paper and other findings of this study are available from the corresponding author upon reasonable request.

References

52. Zhou, S. et al. Dynamic states of swimming bacteria in a nematic liquid crystal cell with homeotropic alignment. *N. J. Phys.* **19**, 055006 (2017).
53. Woolverton, C. J., Gustely, E., Li, L. & Lavrentovich, O. D. Liquid crystal effects on bacterial viability. *Liq. Cryst.* **32**, 417–423 (2005).
54. Dark, M. L., Moore, M. H., Shenoy, D. K. & Shashidhar, R. Rotational viscosity and molecular structure of nematic liquid crystals. *Liq. Cryst.* **33**, 67–73 (2006).
55. Li, B. X., Borshch, V., Shiyanovskii, S. V., Liu, S. B. & Lavrentovich, O. D. Electro-optic switching of dielectrically negative nematic through nanosecond electric modification of order parameter. *Appl Phys. Lett.* **104**, 201105 (2014).
56. Nayani, K., Cordova-Figueroa, U. M. & Abbott, N. L. Steering active emulsions with liquid crystals. *Langmuir* **36**, 6948–6956 (2019).
57. Voloschenko, D., Pishnyak, O. P., Shiyanovskii, S. V. & Lavrentovich, O. D. Effect of director distortions on morphologies of phase separation in liquid crystals. *Phys. Rev. E* **65**, 060701 (2002).
58. Smalyukh, I. I., Shiyanovskii, S. V. & Lavrentovich, O. D. Three-dimensional imaging of orientational order by fluorescence confocal polarizing microscopy. *Chem. Phys. Lett.* **336**, 88–96 (2001).
59. Tinevez, J. Y. et al. TrackMate: an open and extensible platform for single-particle tracking. *Methods* **115**, 80–90 (2017).
60. Thielicke, W. & Stamhuis, E. J. PIVlab—towards user-friendly, affordable and accurate digital particle image velocimetry in MATLAB. *J. Open Res. Softw.* **2**, e30 (2014).

Acknowledgements

We thank B. Li, S. Shiyanovskii and participants of UC Santa Barbara Kavli Institute for Theoretical Physics (KITP) programme 'Active 20: Symmetry, Thermodynamics, and Topology in Active Matter' for fruitful discussions. The work is supported by NSF grants DMR-1905053 (analysis of dynamics), CMMI-1663394 (preparation of plasmonic metamasks for patterned cells), DMS-1729509 (preparation of bacterial dispersions), and by Office of Sciences, DOE, grant DE-SC0019105 (development of the alignment layers). This research was completed while M.R., H.B. and O.D.L. participated in KITP Active 20 programme, supported in part by the NSF grant PHY-1748958 and NIH grant R25GM067110.

Author contributions

M.R. and H.B. performed the experiments, M.R., H.B., T.T. and O.D.L. analysed the data, O.D.L. conceived and supervised the project, M.R. and O.D.L. wrote the manuscript with the input from all co-authors.

Competing interests

The authors declare no competing interests.

Additional information

is available for this paper at https://doi.org/10.1038/s41567-020-01055-5.

Correspondence and requests for materials should be addressed to O.D.L.

Peer review information *Nature Physics* thanks Paulo Arratia, M Cristina and Uroš Tkalec for their contribution to the peer review of this work.

nature research

Corresponding author(s): Oleg D. Lavrentovich

Last updated by author(s): Aug 12, 2020

Reporting Summary

Nature Research wishes to improve the reproducibility of the work that we publish. This form provides structure for consistency and transparency in reporting. For further information on Nature Research policies, see Authors & Referees and the Editorial Policy Checklist.

Statistics

For all statistical analyses, confirm that the following items are present in the figure legend, table legend, main text, or Methods section.

n/a	Confirmed
☐	☒ The exact sample size (*n*) for each experimental group/condition, given as a discrete number and unit of measurement
☐	☒ A statement on whether measurements were taken from distinct samples or whether the same sample was measured repeatedly
☒	☐ The statistical test(s) used AND whether they are one- or two-sided *Only common tests should be described solely by name; describe more complex techniques in the Methods section.*
☒	☐ A description of all covariates tested
☐	☒ A description of any assumptions or corrections, such as tests of normality and adjustment for multiple comparisons
☐	☒ A full description of the statistical parameters including central tendency (e.g. means) or other basic estimates (e.g. regression coefficient) AND variation (e.g. standard deviation) or associated estimates of uncertainty (e.g. confidence intervals)
☒	☐ For null hypothesis testing, the test statistic (e.g. *F*, *t*, *r*) with confidence intervals, effect sizes, degrees of freedom and *P* value noted *Give P values as exact values whenever suitable.*
☒	☐ For Bayesian analysis, information on the choice of priors and Markov chain Monte Carlo settings
☐	☒ For hierarchical and complex designs, identification of the appropriate level for tests and full reporting of outcomes
☒	☐ Estimates of effect sizes (e.g. Cohen's *d*, Pearson's *r*), indicating how they were calculated

Our web collection on statistics for biologists contains articles on many of the points above.

Software and code

Policy information about availability of computer code

Data collection	Data is collected by recording videos using the camera software (Emergent eCapture).
Data analysis	The analysis of the images are done using the TrackMate package of the open source software ImageJ. The calculations and the plots are done using custom written code in Mathematica 12.0, finally the flow inside and outside the droplet is done using the particle image velocimetry, PIVlab MATLAB R2018b.

For manuscripts utilizing custom algorithms or software that are central to the research but not yet described in published literature, software must be made available to editors/reviewers. We strongly encourage code deposition in a community repository (e.g. GitHub). See the Nature Research guidelines for submitting code & software for further information.

Data

Policy information about availability of data

All manuscripts must include a data availability statement. This statement should provide the following information, where applicable:

- Accession codes, unique identifiers, or web links for publicly available datasets
- A list of figures that have associated raw data
- A description of any restrictions on data availability

Source data for Figures 1,2 and 4 are available for this paper. All other data that support the plots within this paper and other findings of this study are available from the corresponding author upon reasonable request

Field-specific reporting

Please select the one below that is the best fit for your research. If you are not sure, read the appropriate sections before making your selection.

☒ Life sciences ☐ Behavioural & social sciences ☐ Ecological, evolutionary & environmental sciences

For a reference copy of the document with all sections, see nature.com/documents/nr-reporting-summary-flat.pdf

Life sciences study design

All studies must disclose on these points even when the disclosure is negative.

Sample size	The sample size was chosen on the idea that an active droplet must contain at least 10 bacteria thus is should be larger than 10 micrometers. On the other hand, the droplet should be smaller than 200 um, because the system will be too dense optically and microscopic observations would be difficult.
Data exclusions	We excluded any data points collected after 30 minutes of filling the cells, to avoid the effects associated with a potential drop of the bacterial activity.
Replication	The results are reproducible, as our error bars are calculated from data of new experiments.
Randomization	The cell thickness is chosen to be about 200 microns; see sample size. Thus the droplet diameter are random within the range 10 micron to 200 microns. The bacteria concentration is chosen high enough to cause motion of the droplets within a measurable time .
Blinding	Two leading co-authors, Hend Baza and Mojtaba Rajabi, performed observations one at a time, i.e. some samples were observed by Hend without Mojtaba, the other samples were observed by Mojtaba without Hend, thus we took blinding precautions and our observations are not biased

Behavioural & social sciences study design

All studies must disclose on these points even when the disclosure is negative.

Study description	The study represent a quantitative description of the active droplets speed dependence on droplets size, bacteria concentration, and does not belong to the field of behavioural and social sciences
Research sample	*State the research sample (e.g. Harvard university undergraduates, villagers in rural India) and provide relevant demographic information (e.g. age, sex) and indicate whether the sample is representative. Provide a rationale for the study sample chosen. For studies involving existing datasets, please describe the dataset and source.*
Sampling strategy	*Describe the sampling procedure (e.g. random, snowball, stratified, convenience). Describe the statistical methods that were used to predetermine sample size OR if no sample-size calculation was performed, describe how sample sizes were chosen and provide a rationale for why these sample sizes are sufficient. For qualitative data, please indicate whether data saturation was considered, and what criteria were used to decide that no further sampling was needed.*
Data collection	*Provide details about the data collection procedure, including the instruments or devices used to record the data (e.g. pen and paper, computer, eye tracker, video or audio equipment) whether anyone was present besides the participant(s) and the researcher, and whether the researcher was blind to experimental condition and/or the study hypothesis during data collection.*
Timing	*Indicate the start and stop dates of data collection. If there is a gap between collection periods, state the dates for each sample cohort.*
Data exclusions	*If no data were excluded from the analyses, state so OR if data were excluded, provide the exact number of exclusions and the rationale behind them, indicating whether exclusion criteria were pre-established.*
Non-participation	*State how many participants dropped out/declined participation and the reason(s) given OR provide response rate OR state that no participants dropped out/declined participation.*
Randomization	*If participants were not allocated into experimental groups, state so OR describe how participants were allocated to groups, and if allocation was not random, describe how covariates were controlled.*

Ecological, evolutionary & environmental sciences study design

All studies must disclose on these points even when the disclosure is negative.

Study description	*Briefly describe the study. For quantitative data include treatment factors and interactions, design structure (e.g. factorial, nested, hierarchical), nature and number of experimental units and replicates.*

Research sample	*Describe the research sample (e.g. a group of tagged Passer domesticus, all Stenocereus thurberi within Organ Pipe Cactus National Monument), and provide a rationale for the sample choice. When relevant, describe the organism taxa, source, sex, age range and any manipulations. State what population the sample is meant to represent when applicable. For studies involving existing datasets, describe the data and its source.*
Sampling strategy	*Note the sampling procedure. Describe the statistical methods that were used to predetermine sample size OR if no sample-size calculation was performed, describe how sample sizes were chosen and provide a rationale for why these sample sizes are sufficient.*
Data collection	*Describe the data collection procedure, including who recorded the data and how.*
Timing and spatial scale	*Indicate the start and stop dates of data collection, noting the frequency and periodicity of sampling and providing a rationale for these choices. If there is a gap between collection periods, state the dates for each sample cohort. Specify the spatial scale from which the data are taken*
Data exclusions	*If no data were excluded from the analyses, state so OR if data were excluded, describe the exclusions and the rationale behind them, indicating whether exclusion criteria were pre-established.*
Reproducibility	*Describe the measures taken to verify the reproducibility of experimental findings. For each experiment, note whether any attempts to repeat the experiment failed OR state that all attempts to repeat the experiment were successful.*
Randomization	*Describe how samples/organisms/participants were allocated into groups. If allocation was not random, describe how covariates were controlled. If this is not relevant to your study, explain why.*
Blinding	*Describe the extent of blinding used during data acquisition and analysis. If blinding was not possible, describe why OR explain why blinding was not relevant to your study.*

Did the study involve field work? ☐ Yes ☒ No

Reporting for specific materials, systems and methods

We require information from authors about some types of materials, experimental systems and methods used in many studies. Here, indicate whether each material, system or method listed is relevant to your study. If you are not sure if a list item applies to your research, read the appropriate section before selecting a response.

Materials & experimental systems

n/a	Involved in the study
☒	☐ Antibodies
☒	☐ Eukaryotic cell lines
☒	☐ Palaeontology
☐	☒ Animals and other organisms
☒	☐ Human research participants
☒	☐ Clinical data

Methods

n/a	Involved in the study
☒	☐ ChIP-seq
☒	☐ Flow cytometry
☒	☐ MRI-based neuroimaging

Antibodies

Antibodies used	*Describe all antibodies used in the study; as applicable, provide supplier name, catalog number, clone name, and lot number.*
Validation	*Describe the validation of each primary antibody for the species and application, noting any validation statements on the manufacturer's website, relevant citations, antibody profiles in online databases, or data provided in the manuscript.*

Eukaryotic cell lines

Policy information about cell lines

Cell line source(s)	*State the source of each cell line used.*
Authentication	*Describe the authentication procedures for each cell line used OR declare that none of the cell lines used were authenticated.*
Mycoplasma contamination	*Confirm that all cell lines tested negative for mycoplasma contamination OR describe the results of the testing for mycoplasma contamination OR declare that the cell lines were not tested for mycoplasma contamination.*
Commonly misidentified lines (See ICLAC register)	*Name any commonly misidentified cell lines used in the study and provide a rationale for their use.*

Palaeontology

Specimen provenance	*Provide provenance information for specimens and describe permits that were obtained for the work (including the name of the issuing authority, the date of issue, and any identifying information).*
Specimen deposition	*Indicate where the specimens have been deposited to permit free access by other researchers.*
Dating methods	*If new dates are provided, describe how they were obtained (e.g. collection, storage, sample pretreatment and measurement), where they were obtained (i.e. lab name), the calibration program and the protocol for quality assurance OR state that no new dates are provided.*

☐ Tick this box to confirm that the raw and calibrated dates are available in the paper or in Supplementary Information.

Animals and other organisms

Policy information about studies involving animals; ARRIVE guidelines recommended for reporting animal research

Laboratory animals	Bacillus subtilis strain 1085.
Wild animals	No wild animals involved.
Field-collected samples	Bacillus subtilis from frozen culture was grown overnight on LB agar at 35C. A colony of the strain was transferred to a vial with 10 mL of Terific Broth solution, then the vial was sealed and grown in a shaking incubator for 7-9 hours. The bacteria concentration in the vial was monitored by measuring the optical scattering and the vial was collected at end of the exponential growth.
Ethics oversight	Kent State University Biohazard and institutional Biosafety Committees

Note that full information on the approval of the study protocol must also be provided in the manuscript.

Human research participants

Policy information about studies involving human research participants

Population characteristics	*Describe the covariate-relevant population characteristics of the human research participants (e.g. age, gender, genotypic information, past and current diagnosis and treatment categories). If you filled out the behavioural & social sciences study design questions and have nothing to add here, write "See above."*
Recruitment	*Describe how participants were recruited. Outline any potential self-selection bias or other biases that may be present and how these are likely to impact results.*
Ethics oversight	*Identify the organization(s) that approved the study protocol.*

Note that full information on the approval of the study protocol must also be provided in the manuscript.

Clinical data

Policy information about clinical studies

All manuscripts should comply with the ICMJE guidelines for publication of clinical research and a completed CONSORT checklist must be included with all submissions.

Clinical trial registration	*Provide the trial registration number from ClinicalTrials.gov or an equivalent agency.*
Study protocol	*Note where the full trial protocol can be accessed OR if not available, explain why.*
Data collection	*Describe the settings and locales of data collection, noting the time periods of recruitment and data collection.*
Outcomes	*Describe how you pre-defined primary and secondary outcome measures and how you assessed these measures.*

ChIP-seq

Data deposition

☐ Confirm that both raw and final processed data have been deposited in a public database such as GEO.

☐ Confirm that you have deposited or provided access to graph files (e.g. BED files) for the called peaks.

Data access links *May remain private before publication.*	*For "Initial submission" or "Revised version" documents, provide reviewer access links. For your "Final submission" document, provide a link to the deposited data.*

Files in database submission	*Provide a list of all files available in the database submission.*
Genome browser session (e.g. UCSC)	*Provide a link to an anonymized genome browser session for "Initial submission" and "Revised version" documents only, to enable peer review. Write "no longer applicable" for "Final submission" documents.*

Methodology

Replicates	*Describe the experimental replicates, specifying number, type and replicate agreement.*
Sequencing depth	*Describe the sequencing depth for each experiment, providing the total number of reads, uniquely mapped reads, length of reads and whether they were paired- or single-end.*
Antibodies	*Describe the antibodies used for the ChIP-seq experiments; as applicable, provide supplier name, catalog number, clone name, and lot number.*
Peak calling parameters	*Specify the command line program and parameters used for read mapping and peak calling, including the ChIP, control and index files used.*
Data quality	*Describe the methods used to ensure data quality in full detail, including how many peaks are at FDR 5% and above 5-fold enrichment.*
Software	*Describe the software used to collect and analyze the ChIP-seq data. For custom code that has been deposited into a community repository, provide accession details.*

Flow Cytometry

Plots

Confirm that:

☐ The axis labels state the marker and fluorochrome used (e.g. CD4-FITC).

☐ The axis scales are clearly visible. Include numbers along axes only for bottom left plot of group (a 'group' is an analysis of identical markers).

☐ All plots are contour plots with outliers or pseudocolor plots.

☐ A numerical value for number of cells or percentage (with statistics) is provided.

Methodology

Sample preparation	*Describe the sample preparation, detailing the biological source of the cells and any tissue processing steps used.*
Instrument	*Identify the instrument used for data collection, specifying make and model number.*
Software	*Describe the software used to collect and analyze the flow cytometry data. For custom code that has been deposited into a community repository, provide accession details.*
Cell population abundance	*Describe the abundance of the relevant cell populations within post-sort fractions, providing details on the purity of the samples and how it was determined.*
Gating strategy	*Describe the gating strategy used for all relevant experiments, specifying the preliminary FSC/SSC gates of the starting cell population, indicating where boundaries between "positive" and "negative" staining cell populations are defined.*

☐ Tick this box to confirm that a figure exemplifying the gating strategy is provided in the Supplementary Information.

Magnetic resonance imaging

Experimental design

Design type	*Indicate task or resting state; event-related or block design.*
Design specifications	*Specify the number of blocks, trials or experimental units per session and/or subject, and specify the length of each trial or block (if trials are blocked) and interval between trials.*
Behavioral performance measures	*State number and/or type of variables recorded (e.g. correct button press, response time) and what statistics were used to establish that the subjects were performing the task as expected (e.g. mean, range, and/or standard deviation across subjects).*

Acquisition

Imaging type(s) — *Specify: functional, structural, diffusion, perfusion.*

Field strength — *Specify in Tesla*

Sequence & imaging parameters — *Specify the pulse sequence type (gradient echo, spin echo, etc.), imaging type (EPI, spiral, etc.), field of view, matrix size, slice thickness, orientation and TE/TR/flip angle.*

Area of acquisition — *State whether a whole brain scan was used OR define the area of acquisition, describing how the region was determined.*

Diffusion MRI ☐ Used ☐ Not used

Preprocessing

Preprocessing software — *Provide detail on software version and revision number and on specific parameters (model/functions, brain extraction, segmentation, smoothing kernel size, etc.).*

Normalization — *If data were normalized/standardized, describe the approach(es): specify linear or non-linear and define image types used for transformation OR indicate that data were not normalized and explain rationale for lack of normalization.*

Normalization template — *Describe the template used for normalization/transformation, specifying subject space or group standardized space (e.g. original Talairach, MNI305, ICBM152) OR indicate that the data were not normalized.*

Noise and artifact removal — *Describe your procedure(s) for artifact and structured noise removal, specifying motion parameters, tissue signals and physiological signals (heart rate, respiration).*

Volume censoring — *Define your software and/or method and criteria for volume censoring, and state the extent of such censoring.*

Statistical modeling & inference

Model type and settings — *Specify type (mass univariate, multivariate, RSA, predictive, etc.) and describe essential details of the model at the first and second levels (e.g. fixed, random or mixed effects; drift or auto-correlation).*

Effect(s) tested — *Define precise effect in terms of the task or stimulus conditions instead of psychological concepts and indicate whether ANOVA or factorial designs were used.*

Specify type of analysis: ☐ Whole brain ☐ ROI-based ☐ Both

Statistic type for inference (See Eklund et al. 2016) — *Specify voxel-wise or cluster-wise and report all relevant parameters for cluster-wise methods.*

Correction — *Describe the type of correction and how it is obtained for multiple comparisons (e.g. FWE, FDR, permutation or Monte Carlo).*

Models & analysis

n/a	Involved in the study
☐	☐ Functional and/or effective connectivity
☐	☐ Graph analysis
☐	☐ Multivariate modeling or predictive analysis

Functional and/or effective connectivity — *Report the measures of dependence used and the model details (e.g. Pearson correlation, partial correlation, mutual information).*

Graph analysis — *Report the dependent variable and connectivity measure, specifying weighted graph or binarized graph, subject- or group-level, and the global and/or node summaries used (e.g. clustering coefficient, efficiency, etc.).*

Multivariate modeling and predictive analysis — *Specify independent variables, features extraction and dimension reduction, model, training and evaluation metrics.*